

## Origin of Difference between $\bar{u}$ and $\bar{d}$ Partons in the Nucleon

Keh-Fei Liu and Shao-Jing Dong

*Department of Physics and Astronomy, University of Kentucky, Lexington, Kentucky 40506*

(Received 28 April 1993; revised manuscript received 10 September 1993)

Using the Euclidean path-integral formulation for the hadronic tensor, we show that the large difference between  $\bar{u}$  and  $\bar{d}$  does not come from the disconnected quark-loop insertion. Rather, it can come from the connected (quark line) insertion involving quarks propagating backwards in time. We study the influence of the backward time propagator in the axial-vector and scalar matrix elements in lattice gauge calculations and give an estimate of the violation of the Gottfried sum rule.

PACS numbers: 13.60.Hb, 11.55.Hx, 12.38.Gc, 14.20.Dh

A recent measurement of the first moment of the difference between the proton and neutron structure functions, i.e.,  $S_G = \int_0^1 dx [F_2^p(x) - F_2^n(x)]/x$ , by the New Muon Collaboration (NMC) [1], has shown a surprising disagreement with the expectation of the naive parton model. Assuming charge or isospin symmetry,  $S_G$  can be expressed in terms of the parton distributions as  $S_G = 1/3 + 2/3 \int_0^1 dx [\bar{u}^p(x) - \bar{d}^p(x)]$ . The naive parton model which assumes isospin symmetry in the "sea," i.e.,  $\bar{u}^p(x) = \bar{d}^p(x)$ , leads to the Gottfried sum rule (GSR),  $S_G = 1/3$  [2]. Yet, the NMC data give  $S_G = 0.24 \pm 0.016$ , which implies that  $\bar{u}^p(x)$  and  $\bar{d}^p(x)$  are not the same in the proton with the number of  $\bar{u}^p$  less than that of  $\bar{d}^p$ .

This has generated a good deal of theoretical interest. The apparent isospin asymmetry in the parton distribution was envisioned by Field and Feynman [3] as due to the Pauli principle and has been modeled [4] with the Sullivan process [5] which considers the meson cloud in the nucleon and the chiral-quark model [6].

In this Letter, we shall examine the origin of this large  $\bar{u}/\bar{d}$  difference in the Euclidean path integral formulation of the hadronic tensor. We show that the large  $\bar{u}/\bar{d}$  difference does not come from the quark-loop insertion, but may originate from the connected insertion with

quarks propagating backwards in time between the currents. The importance of this effect is then illuminated in the axial and scalar matrix elements through lattice calculations. Finally, we give an estimate of the violation of the GSR via the valence approximation in which the backward time propagator is explicitly eliminated.

The deep inelastic scattering of muon on nucleon involves the hadronic tensor of the current-current correlation function in the nucleon, i.e.,

$$W_{\mu\nu}(q^2, \nu) = \frac{1}{2M_N} \left\langle N \left| \int \frac{d^4x}{2\pi} e^{iq \cdot x} J_\mu(x) J_\nu(0) \right| N \right\rangle_{\text{spin ave}}$$

This forward Compton amplitude can be obtained by considering the ratio of the four-point function  $\langle O_N(t) J_\mu(\mathbf{x}, t_1) J_\nu(0, t_2) O_N(0) \rangle$  and the two-point function  $\langle O_N(t - (t_1 - t_2)) O_N(0) \rangle$ , where  $O_N(t)$  is the zero-momentum interpolation field for the nucleon at Euclidean time  $t$ .

As both  $t - t_1 \gg 1/\Delta M_N$  and  $t_2 \gg 1/\Delta M_N$ , where  $\Delta M_N$  is the mass gap between the nucleon and the next excitation (i.e., the threshold of a nucleon and a pion in the  $p$  wave), the intermediate state contributions will be dominated by the nucleon with the Euclidean propagator  $e^{-M_N[t - (t_1 - t_2)]}$ . Hence,

$$\begin{aligned} \widetilde{W}_{\mu\nu}(\mathbf{q}^2, \tau) &= \frac{1}{2M_N} \frac{\langle O(t) \int \frac{d^3x}{2\pi} e^{-i\mathbf{q} \cdot \mathbf{x}} J_\mu(\mathbf{x}, t_1) J_\nu(0, t_2) O(0) \rangle}{\langle O(t - \tau) O(0) \rangle} \Bigg|_{t - t_1, t_2 \gg 1/\Delta M_N} \\ &= \frac{1}{2M_N V} \left\langle N \left| \int \frac{d^3x}{2\pi} e^{-i\mathbf{q} \cdot \mathbf{x}} J_\mu(\mathbf{x}, t_1) J_\nu(0, t_2) \right| N \right\rangle, \end{aligned} \quad (1)$$

where  $\tau = t_1 - t_2$  and  $V$  is the 3-volume. The hadronic tensor can be obtained formally by the inverse Laplace transform [7],  $W_{\mu\nu}(q^2, \nu) = \frac{V}{i} \int_{c-i\infty}^{c+i\infty} d\tau e^{\nu\tau} \widetilde{W}_{\mu\nu}(\mathbf{q}^2, \tau)$  or through an appropriate fitting procedure in practice.

In the Euclidean path-integral formulation, the four-point function can be classified according to different topologies of the quark paths between the source and the sink of the proton. They represent different ways the fields in the currents  $J_\mu$  and  $J_\nu$  contract with those in the nucleon interpolation operator  $O_N$  at different times. This is so because the quark action and the electromagnetic currents are both bilinear in quark fields, i.e., in the

form of  $\bar{\Psi} M \Psi$ , so that the quark numbers are conserved and as a result the quark line does not branch the way a gluon line does. As illustrated in Fig. 1, we see (a) and (b) represent connected insertions (CI) where the quark fields from the currents contract with those from  $O_N$  and the quark lines from  $t = 0$  to  $t = t$  are thus connected with the currents. Figure 1(c), on the other hand, represents a disconnected insertion (DI) where the quark fields from  $J_\mu$  and  $J_\nu$  self-contract and are hence disconnected from the quark paths between the proton source and sink. Here, "disconnected" refers only to the quark lines. Of

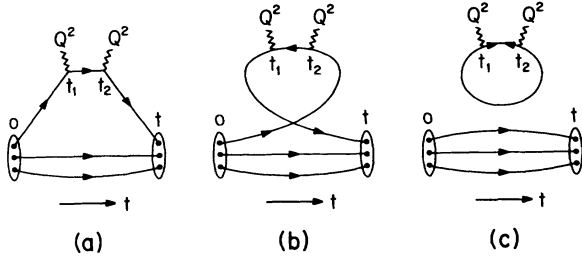


FIG. 1. Time-ordered "handbag" skeleton diagrams of quark lines with different topologies. (a) [(b)] is the CI involving a quark [antiquark] propagator between the currents. (c) is a DI involving sea quarks and antiquarks.

course, quarks sail in the background of the gauge field and all quark paths are ultimately connected through the gluon lines. The infinitely many possible gluon lines and additional quark loops are implicitly there in Fig. 1 but are not explicitly drawn. Figure 1 represents the contributions of the class of "handbag" diagrams where the two currents are hooked on the same quark line. These are leading twist contributions in deep inelastic scattering. The other possible contractions are those diagrams where the two currents are hooked onto different quark lines. Given a renormalization scale, these are higher twist contributions in the Bjorken limit. We shall neglect these "cat's ears" diagrams in the following discussion.

In the deep inelastic limit where  $x^2 \leq O(1/Q^2)$  (we are using the Minkowski notation here), the leading light-cone singularity of the current product (or commuta-

tor) gives rise to free quark propagator between the currents. In the time-ordered diagrams in Fig. 1, (a) [(b)] involves only quark [antiquark] propagator between the currents, while (c) has both quark and antiquark propagators. Hence, there are two distinct classes of diagrams where the antiquarks contribute. One comes from the DI; the other comes from the CI. It is frequently assumed that connected insertions involve only "valence" quarks which are responsible for the baryon number. Apparently, this is not true. To define the quark distribution functions more precisely, we shall call the antiquark distribution from the DI, which are connected to the other quark lines through gluons, the "sea" antiquarks and the antiquarks from the CI the "cloud" antiquarks. Thus, in the parton model, the antiquark distribution should be written as

$$\bar{q}^i(x) = \bar{q}_c^i(x) + \bar{q}_s^i(x) \tag{2}$$

to denote their respective origins of Fig. 1(b) and Fig. 1(c) for each flavor  $i$ . Similarly, the quark distribution is written as

$$q^i(x) = q_V^i(x) + q_c^i(x) + q_s^i(x), \tag{3}$$

where  $q_s^i(x)$  comes from Fig. 1(c) and both  $q_V^i(x)$  and  $q_c^i(x)$  are from Fig. 1(a). Since  $q_s^i(x) = \bar{q}_s^i(x)$ , we define  $q_c^i(x) = \bar{q}_c^i(x)$  so that  $q_V^i(x)$  will be responsible for the baryon number, i.e.,  $\int u_V(x) dx = \int [u(x) - \bar{u}(x)] dx = 2$  and  $\int d_V(x) dx = \int [d(x) - \bar{d}(x)] = 1$  for the proton.

We shall first examine Fig. 1(c). After the integration of the Grassman fields  $\Psi$  and  $\bar{\Psi}$ , the path integral for Fig. 1(c) can be written as the correlated part of

$$\int D[A] e^{-S_G} \text{Tr}[M^{-1}(t_2, t_1) \gamma_\nu M^{-1}(t_1, t_2) \gamma_\mu] \text{Tr}[M^{-1}(t, 0) \dots M^{-1}(t, 0) \dots M^{-1}(t, 0) \dots], \tag{4}$$

where  $A$  is the gluon field,  $S_G$  the gluon action, and  $M$  is the quark matrix in the bilinear quark action  $\bar{\Psi} M \Psi$ .  $M^{-1}(t_1, t_2)$  denotes the quark propagator from  $t_2$  to  $t_1$ . Note in Eq. (4), the trace is over the flavor as well as the color-spin indices. Since the quark loop involving the currents is separately traced from those quark propagators  $M^{-1}(t, 0)$  whose trace reflects the quantum numbers of the proton, Eq. (4) does not distinguish a loop with the  $u$  quark from that with the  $d$  quark at the flavor-symmetric limit, i.e.,  $m_u = m_d$ . These are referred to as sea quarks/antiquarks in the naive parton model, since they are connected to those quarks which generate the hadron state via the gluon lines. These sea quarks cannot give rise to the violation of the GSR, since Eq. (4) infers  $\bar{u}_s = \bar{d}_s$ . The isospin breaking will give a small effect in the order of  $(m_u - m_d)/M_c$  [8], where  $M_c$  is the constituent quark mass which reflects the confinement scale. Hence, the isospin symmetry breaking effect will be at the 1% level. It cannot explain the violation of the GSR which is at  $\sim 30\%$  level [1]. On the other hand, the antiquark propagator connecting the currents in Fig. 1(b) shows up in the same trace along with other quark propagators connecting the interpolation fields. There-

fore, the cloud antiquarks are subjected to the Pauli exclusion as are the valence quarks and cloud quarks in Fig. 1(a) [9]. Consider the Fock space where a  $u$  quark line does the twisting in Fig. 1(b), the simplest Fock space would then be  $uuu\bar{u}d$ . With three  $u$  quarks, this Fock space configuration might be more Pauli suppressed than the corresponding Fock space of  $uudd\bar{d}$  with two  $u$  quarks and two  $d$  quarks. We believe this is the reason for the large  $\bar{d}/\bar{u}$  difference in the nucleon as revealed by the NMC data. Consequently, neglecting the isospin symmetry breaking, the sum  $S_G$  can be written as

$$S_G = \frac{1}{3} + \frac{2}{3} \int_0^1 dx [\bar{u}_c(x) - \bar{d}_c(x)], \tag{5}$$

which shows that the violation of GSR comes mainly from the cloud antiquarks.

Equation (5) could be verified if one evaluates the hadronic tensor directly. Unfortunately, it is too numerically intensive a task. Instead, we shall calculate matrix elements with one current which involve three-point functions. In the spirit of the operator product expansion (OPE), matrix elements of certain twist-2 operators are

the sum rules of the parton distributions. This can be viewed as when  $x^2 \rightarrow 0$  in the Bjorken limit, the two currents at  $t_1$  and  $t_2$  merge into one so that the connected insertion of one local operator will have both types of paths represented in Figs. 1(a) and 1(b). In fact, there has been indirect evidence of the cloud antiquarks in previous studies of three-point functions in quenched lattice QCD calculations, such as the  $\rho$  meson dominance in the pion electric form factor [10] and the negative neutron charge radius [11]. However, the first moment of the structure function  $F_2$  which we are interested in is not expressible in terms of the forward matrix element of a twist-2 operator; hence we will not be able to calculate the sum  $S_G$  in Eq. (5) directly. Nevertheless, we can explicitly reveal the existence and influence of the cloud antiquark in the axial-vector and scalar matrix elements which are also sensitive to its presence. From the OPE, the isovector  $g_A^3$  from the forward axial current matrix element is related to the Bjorken sum rule of the polarized parton distribution; so is  $g_A^1$  related to a flavor-singlet sum rule. These matrix elements involve both the CI and the DI (in the isospin symmetric case, the DI cancels out for the isovector  $g_A^3$ ). Since we are interested only in the cloud quark effects which are in the CI, we shall not be concerned with the DI part. To reduce lattice corrections like the finite volume effect, scaling, and finite lattice renormalization, we shall consider ratios of matrix elements. From the OPE and the parton model, the ratio of the isoscalar to isovector axial matrix element (or  $g_A$ ) for the CI can be written as

$$R_A = \frac{g_A^1}{g_A^3} \Big|_{\text{CI}} = \frac{\int dx [\Delta u(x) + \Delta d(x)]}{\int dx [\Delta u(x) - \Delta d(x)]} \Big|_{\text{CI}}, \quad (6)$$

where  $\Delta u$  ( $\Delta d$ ) is the polarized parton distribution of the  $u$  ( $d$ ) quark and antiquark in the CI [i.e., from Figs. 1(a) and 1(b)]. For the nonrelativistic case,  $g_A^3$  is  $5/3$  and  $g_A^1$  for the CI is 1 (the spin of the proton is entirely carried by the quarks in this case) [12]. Thus, the ratio  $R_A$  should be  $3/5$ . Our lattice results based on quenched  $16^3 \times 24$  lattices with  $\beta = 6$  for the Wilson  $\kappa$  ranging between 0.154 to 0.105 which correspond to strange and twice the charm masses are plotted in Fig. 2. We indeed find this ratio for the heavy quarks (i.e.,  $\kappa \geq 0.133$  or  $m_q a \geq 0.4$  in Fig. 2). This is to be expected because the cloud antiquarks which involve  $Z$  graphs are suppressed for nonrelativistic quarks by  $O(p/m_q)$ . Interestingly, the ratio dips under  $3/5$  for light quarks. We interpret this as due to the cloud quark and antiquark, since in the relativistic valence quark models (i.e., no cloud nor sea quarks) the ratio remains  $3/5$ . To verify that this is indeed caused by the cloud antiquarks from the backward time propagation, we perform the following approximation. In the Wilson lattice action, the backward time hopping is prescribed by the term  $-\kappa(1 - \gamma_4)U_4(x)\delta_{x,y-a_4}$ . We shall amputate this term from the quark matrix in our calculation of the quark propagators. As a result, the quarks are limited to prop-

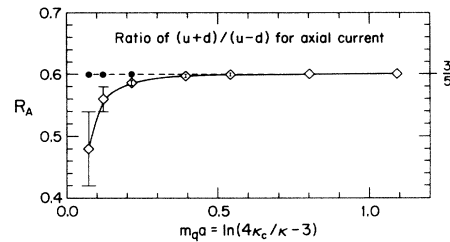


FIG. 2. The ratio of the isoscalar to isovector  $g_A$  of the proton for the CI (shown as  $\diamond$ ) vs quark mass  $m_q a$ .

agating forward in time and there will be no  $Z$  graph and hence no cloud quarks and antiquarks. The Fock space is limited to three valence quarks. Thus we shall refer to this as the *valence approximation* and we believe it simulates what the naive quark model is supposed to delineate by design. After making this valence approximation for the light quarks with  $\kappa = 0.148, 0.152$ , and  $0.154$ , we find that the ratio  $R_A$  becomes  $3/5$  with errors less than the size of the dots in Fig. 2. We should point out that the quark mass in the valence approximation, although the same as before at the tree and tadpole levels, can differ from that of the quenched approximation at the perturbative one-loop order, i.e.,  $O(\alpha_s)$ , which is presumably small for Wilson fermions [13]. We have verified this by calculating the pseudoscalar meson masses. For the quenched approximation, these masses in lattice units are 0.689(6), 0.493(7), and 0.385(9) for  $\kappa = 0.148, 0.152$ , and  $0.154$ , respectively. The corresponding masses in the valence approximation are 0.668(12), 0.486(5), and 0.393(16). Thus we see, except for  $\kappa = 0.148$ , the pseudoscalar meson masses are the same within errors. The  $\kappa_c$ , determined from the extrapolation of the pion mass to zero, is 0.1568(1)/0.1571(2) for the quenched/valence approximation. Taking the central values for these  $\kappa_c$ , the quark mass  $m_q a = \ln(4\kappa_c/\kappa - 3)$  for  $\kappa = 0.154$  is then increased by 10% in the valence approximation from that of the quenched approximation. Since this is only about 12 MeV, we have neglected this small mass difference in Fig. 2 and the subsequent Fig. 3 and used the same  $\kappa_c = 0.1568$ . Since the valence quark model prediction of  $R_A$  is well reproduced by the valence approximation, we believe this proves our point that the deviation of  $R_A$  from  $3/5$  in Fig. 2 is caused by the backward time propagation, i.e., the cloud quarks and antiquarks.

We have also examined the scalar matrix elements. The scalar charge expanded in the plane-wave basis

$$\int d^3x \bar{\Psi}\Psi(x) = \int d^3k \frac{m}{E} \sum_s [b_{k,s}^\dagger b_{k,s} + d_{k,s}^\dagger d_{k,s}] \quad (7)$$

is the sum of the quark and antiquark numbers weighted by the factor  $m/E$ . To the extent that the  $m/E$  factor does not have a large dispersion (we shall come back to this point later), the scalar matrix element has been taken as a measure of the quark and antiquark numbers [14]. In the parton model description of the forward

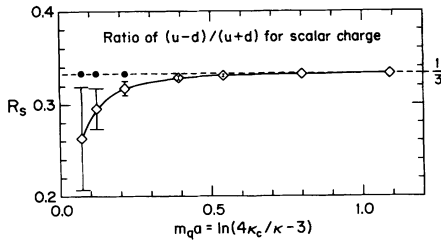


FIG. 3. The same as in Fig. 2 for the ratio of the isovector to isoscalar scalar charge  $R_S$ .

matrix element, the ratio of the isovector to isoscalar scalar charge of the proton for the CI is then approximated according to Eqs. (2) and (3) as

$$R_S = \frac{\langle p | \bar{u}u - \bar{d}d | p \rangle}{\langle p | \bar{u}u + \bar{d}d | p \rangle} \Big|_{\text{CI}} = \frac{1 + 2 \int dx [\bar{u}_c(x) - \bar{d}_c(x)]}{3 + 2 \int dx [\bar{u}_c(x) + \bar{d}_c(x)]}. \quad (8)$$

Since the quark/antiquark number is positive definite, we expect this ratio to be  $\leq 1/3$ . For heavy quarks where the cloud antiquarks are suppressed, the ratio is indeed  $1/3$  (see Fig. 3). For quarks lighter than  $\kappa = 0.140$ , we find that the ratio is in fact less than  $1/3$ . We take this to be the evidence of the cloud antiquarks in Eq. (8). To the extent the factor  $m/E$  can be approximated by a constant factor, the ratio  $R_S$  in Eq. (8) should be  $1/3$  in the valence approximation. The lattice results of the valence approximation for the light quarks, shown as the dots in Fig. 3, indeed turn out to be  $1/3$ . This shows that the deviation of  $R_S$  from  $1/3$  is caused by the cloud quarks and antiquarks. In retrospect, this can also be used to justify approximating  $m/E$  by a constant factor in Eq. (8). With these findings, we can give an upper bound for the violation of GSR. The prediction that  $R_A = 3/5$  and  $R_S = 1/3$  in the relativistic quark model is based on the assumption that the valence quarks move in a single orbital with totally symmetric spatial wave function so that the ratio  $3/5$  for  $R_A$  is purely determined by the flavor-spin  $SU(6)$  group and  $R_S = 1/3$  reflects the valence quark ratio with the common  $m/E$  factor dropped out. Since the lattice calculation for the valence approximation (no cloud) reproduces these ratios accurately, we interpret this to imply that the valence quarks do move in a single orbital with a definite  $E$  as in the quark model. To go back to the case with the cloud, the Fock space components with cloud  $q\bar{q}$  pairs will have higher energies than that of the lowest component with valence only. From this we can derive an upper bound for the  $\bar{u} - \bar{d}$  number in the proton. Expressing Eq. (7) in terms of the sum over quark orbital basis, we obtain  $n_{\bar{u}} - n_{\bar{d}} \leq \frac{1}{2} [\langle N | \bar{u}u - \bar{d}d | N \rangle_{\text{cloud}} / \langle N | \bar{u}u - \bar{d}d | N \rangle_{\text{valence}} - 1]$ . This way we have divided out the  $m/E$  factor and the finite lattice renormalization assuming that the latter is the same in both cases. Our lattice result extrapolated to the chiral limit gives  $n_{\bar{u}} - n_{\bar{d}} \leq -0.12 \pm 0.05$ . This clearly shows that  $n_{\bar{u}} - n_{\bar{d}}$  is negative and is quite consistent with the experimental result  $\int dx [\bar{u}^p(x) - \bar{d}^p(x)] = -0.14 \pm 0.024$ .

There are phenomenological consequences for the cloud quarks. Since strange and charm quarks come only from the sea in Fig. 1(c), it is natural to expect that  $\bar{u}, \bar{d} > \bar{s}, \bar{c}$  since the  $\bar{u}$  and  $\bar{d}$  have both the sea and cloud parts. The violation of the GSR has been modeled in terms of the Sullivan process [4] and the chiral quark model [6]. Although these models give the right picture in terms of the cloud antiquarks, they do not distinguish the two topological possibilities in Figs. 1(b) and 1(c).

In conclusion, we have shown in the Euclidean path-integral formalism that the large experimentally observed  $\bar{d}/\bar{u}$  difference in the proton comes from the CI which involves cloud quarks and antiquarks. We have studied it in the ratios of the isovector to isoscalar axial and scalar charges of the proton in lattice calculations. We found that these ratios have the expected nonrelativistic and relativistic behaviors as far as the cloud antiquarks are concerned. We demonstrate this by truncating the quark backward time propagation which then leads to the valence quark model predictions.

This work is supported in part by the DOE Grant No. DE-FG05-84ER40154. The authors would like to thank S.J. Brodsky, G.E. Brown, N. Christ, T. Draper, G. Garvey, J.C. Peng, M. Rho, W. Wilcox, and R.M. Woloshyn for discussions. They also thank S. Brodsky for pointing out that a classification similar to the CI and DI has been discussed by Brodsky and Schmidt [15].

- [1] New Muon Collaboration, P. Amaudruz *et al.*, Phys. Rev. Lett. **66**, 2712 (1991).
- [2] K. Gottfried, Phys. Rev. Lett. **18**, 1174 (1967).
- [3] R.D. Field and R.P. Feynman, Phys. Rev. D **15**, 2590 (1977).
- [4] S. Kumano, Phys. Rev. D **43**, 59 (1991); **43**, 3067 (1991); E.M. Henley and G.A. Miller, Phys. Lett. B **251**, 453 (1990); A. Siganl, A.W. Schreiber, and A.W. Thomas, Mod. Phys. Lett. A **6**, 271 (1991); W.-Y. P. Hwang, J. Speth, and G.E. Brown, Z. Phys. A **339**, 383 (1991).
- [5] J.D. Sullivan, Phys. Rev. D **5**, 1732 (1972).
- [6] E. Eichten, I. Hinchliffe, and C. Quigg, Phys. Rev. D **45**, 2269 (1992).
- [7] W. Wilcox, Nucl. Phys. (Proc. Suppl.) **B30**, 491 (1993).
- [8] D.J. Gross, S.B. Treiman, and F. Wilczek, Phys. Rev. D **19**, 2188 (1979).
- [9] To state it in another way, any Pauli exchange diagram between the sea quark/antiquark and those quarks/antiquarks connecting the interpolating fields in Fig. 1(c) will inevitably end up in the CI in Fig. 1(a) or 1(b), whereas the Pauli exchange diagrams of the CI can still be in the class of the CI.
- [10] T. Draper, R.M. Woloshyn, K.F. Liu, and W. Wilcox, Nucl. Phys. **B318**, 319 (1989).
- [11] W. Wilcox, T. Draper, and K.F. Liu, Phys. Rev. D **46**, 1109 (1992).
- [12] K.F. Liu, Phys. Lett. B **281**, 141 (1992).
- [13] P. MacKenzie, in Proceedings of the Lattice '93 Conference, Dallas, 1993 (to be published).
- [14] S. Forte, Phys. Rev. D **47**, 1842 (1993).
- [15] S. J. Brodsky and I. Schmidt, Phys. Rev. D **43**, 179 (1991).